The effect of different carrier fluids on heat transfer performance in a microfluidic serpentine device

Jais Mohamed*, Michela Spizzichino, Giovanni Paolo Romano,

Department of Mechanical and Aerospace Engineering, University of Rome La Sapienza, Italy

* Email: jais.mohamed@uniroma1.it

Abstract: In this work, the efficiency of heat transfer and the related fluid-mechanic performance inside a microfluidic device are investigated by varying the type of carrier fluid at different flow rates. The experimental analysis has been conducted on a serpentine channel configuration by considering five different fluid mixtures. The results displayed and emphasized the relevant role of viscosity on thermal performance in the laminar regime. The corresponding Nusselt number values have been identified in terms of Reynolds and Prandtl numbers. Viscous mixtures have exhibited Nusselt number values highly correlated with Prandtl number. Nusselt-Reynolds trends for such mixtures have also presented a consistent rate of increase. However, this increment is severely limited by the action of viscous dissipation as Reynolds number increases. Mixtures with lower viscosity showed a higher correlation between Nusselt and Reynolds numbers. The importance of local turbulence phenomena for low-viscosity fluids becomes one of the main factors in heat transfer enhancement, also for small-scale thermal sinks in laminar regime.

Keywords: Micro-serpentine, Carrier mixtures comparison, Thermal efficiency, Micro-PIV

1. Introduction

Microfluidic devices gained significant amount of interest in recent years through the studies of phenomenology and applications regarding heat transport. In fact, considering that convection is the main heat transfer mechanism regulating efficiency of these devices, and since the convection coefficient is inversely related to the size of the micro-channel, a valid solution to optimize the cooling process is to connect several microfluidic devices rather than a single standard size one [1]. This statement could explain why many early studies on heat transfer efficiency in microfluidic devices was mainly focused on the influence of geometrical parameters. One of the marked aspects treated was the scaling of hydraulic diameters of microfluidic devices as performed by Pfahler *et a*l [2]. An

Nomenclature

Geometrical Parameters

D	Hydraulic equivalent diameter
S	Section of square channel
A	Heat transfer area
L	Length of square channel

Constitutive Fluid-Mixture Parameters

ρ	Density
c_p	Specific heat coefficient
μ	Dynamic viscosity
λ	Thermal conductivity
α_T	Thermal diffusivity
v	Kinematic viscosity
x_v	Volumetric concentration
x_m	Mass concentration

Kinematic Parameters

u	Mean axial velocity
v	Mean cross velocity
m	Mean velocity magnitude
ω	Mean vorticity orthogonal component

Experimental Parameters

T_w	Heated wall temperature
T_p	Hot Plate temperature
T_{in}	Inlet temperature
T_{out}	Outlet temperature
T_{bulk}	Bulk temperature
T_∞	Asymptotic outlet temperature
Q	Flow rate
Δp	Pressure losses

Dimensionless Output Parameters

Re	Reynolds number
Pr	Prandtl number
Gz	Graetz number
Nu	Nusselt number
Br	Brinkman number
f	Friction factor
$\varepsilon, \varepsilon'$	Thermal Efficiencies

Statistical Estimators

R^2	Coefficient of determination
σ_{rms}	Root mean square error of regression
$\alpha,\beta,\gamma,\delta,\eta$	Estimators of regression coefficients

increasing loss of accuracy was observed by applying fluid-kinetic models derived from the use of the Navier-Stokes equations as the diameter of the considered micro-channel decreased. Regarding the importance of diameters scale, Mehendale *et al* [3] and Kandlikar and Grande [4] proposed a classification in terms of compactness of channels and type of heat sink, respectively. The importance of geometry in microdevices is also linked to the presence of significant pressure drops [5]. Related to this latter, the choice of micro-channel shape is the first aspect to be considered. Many different configurations [6][7][8] have been studied to evaluate the thermal performance of each geometry, as

quantified by the Nusselt number and the friction factor. In all these works, it has been shown that the convective heat transfer can be enhanced in the laminar regime by activating recirculating flows and extended vortical regions. These vortices increase the mixing in curved sections of micro and mini channels, as reported. However, as previously stated, the presence of curvatures and geometrical complexities in small-scale channels also induces a large increase in pressure losses. As a result, more energy costs would be required to pump the fluid if compared to a flow within a straight micro-channel. In any case, Sui *et al* [7] have demonstrated that in wavy shaped micro-channels, heat transfer enhancement in terms of Nusselt number is larger than the pressure drop increase, even if this conclusion must be supported in each specific configuration. To evaluate this balance between an increase of useful thermal effects and enhancements in energy costs, Alok *et al* [9] carried out a formulation to quantify the thermal efficiency of a thermofluidic system. This approach in performance criteria evaluation has been applied by Rastan *et al* [10] in the study of additively manufactured microchannel heat exchangers. In this framework, Spizzichino *et al* [11] carried out an experimental study to identify the best geometry in terms of thermal efficiency as defined by [9]. In the aforementioned work, parallel channels, wavy channels, as in [7], and standard serpentine channels [12] were the investigated configurations. Said study has identified the standard serpentine as the device with the highest efficiency by varying the flow rate of the distilled water. So far, the effect of geometry on convective heat transfer must be evaluated based on the flow regime and of the resulting pressure drop. This indicates that the effects of employing different geometries are retained in the correlation between Nusselt number, friction factor and Reynolds number. As it is well known from Buckingham's analysis [13], convection phenomenology and therefore Nusselt number are strongly related to the chemical-physical nature of the cooling fluid. In fact, in addition to Reynolds number, Nusselt correlation also includes Prandtl number [14][15], and Brinkman number [16] as non-dimensional parameters. These last two dimensionless groups are changed mainly by considering the constitutive properties of the cooling fluid. A consistent number of correlations has been introduced in order to correlate Nusselt number to all aforementioned dimensionless groups, as Lee *et al* [17] have illustrated. One of the milestone correlations is reported in detail in the work of Sieder&Tate [18]. In this latter study, heat transfer and thus Nusselt number are affected also by the variation of dynamic viscosity as a function of temperature. The introduction of dynamic viscosity ratio at bulk and heated-wall temperatures as a factor into Nusselt number correlations [19] was followed in several other subsequent works [20][21]. Sieder&Tate correlation continues to be one of the main benchmarks for internal forced convection studies, including mini and microfluidic studies [10][11][21]. With reference to Brinkman number, the magnitude evaluation of this dimensionless number turns out to be an important factor especially in the presence of highly viscous fluids. Tso

and Mahulikar [22] have shown how the presence of viscous dissipation in the laminar regime within micro-channels can increase carrier fluid temperature to such an extent that heat transfer between fluid and the heated walls would drop in performance. If the presence of an increasing viscous dissipation would raise the fluid temperature to a value greater than that of the heated walls by rising Reynolds number, negative Nusselt numbers would be obtained [22]. In summary, the comprehensive study of small-scale devices with state-of-the-art geometrical configurations also requires an evaluation of its performance for different cooling fluids. Therefore, in the present work, the effect of different carrier cooling mixtures on heat transfer in a microfluidic standard serpentine is investigated from an experimental point of view. Five different types of liquid mixtures have been considered, which allow varying physical properties of the fluid flow in a rather large range. Results in terms of thermal efficiency for each mixture will be presented to give quantitative comparisons of results, also considering the contribution of other relevant dimensionless groups. In parallel, detailed flow field measurements, using Micro Particle Image Velocimetry (μPIV) are provided to give insights on the phenomena responsible for performance improvements.

2. The Experimental Set-Up

The microfluidic cell used in this work is the same serpentine channel already investigated in a previous paper [11]. This cell is sketched in Figure 1 and is composed by two essential parts: an aluminium base which is directly in contact with the hot source during the measurements and a Plexiglas top side in which the channel is milled. The whole structure is kept together by screws and a hydraulic seal is inserted in the middle of the two parts. The total length of the device is 120 mm, its width is 50 mm and thickness of 22 mm, 10 mm corresponding to the height of the Plexiglas panel housing the channel and the remaining 12 mm to the aluminium base. The latter is higher than the Plexiglas layer in order to have additional space for 1.5 mm holes used to measure the local temperature of the basement through K-type thermocouples. The channel has a 1 x 1 mm^2 square

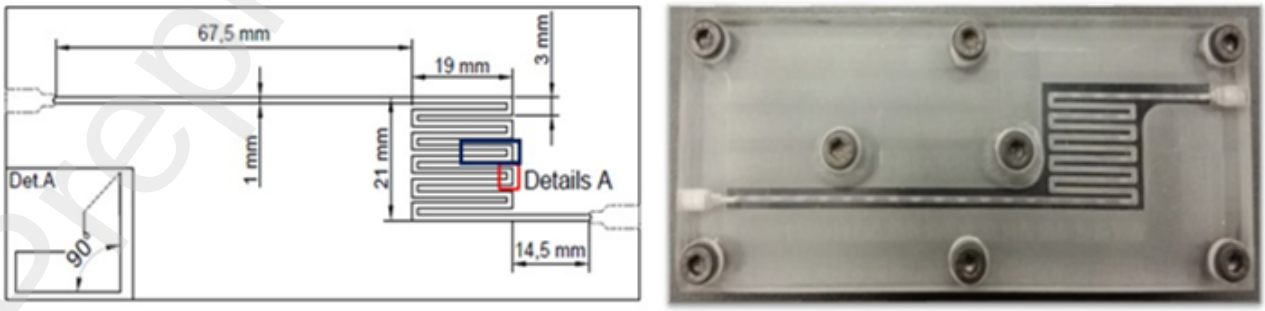

Figure 1: Blueprint (left) and actual photo (right) of the investigated standard serpentine micro-device.

cross section and an equivalent length of 297 mm. The cell consists of eleven horizontal linear channels each one with a length of 19 mm, followed by a U-shaped channel with a 90° angle inversion, each one with a length of 3 mm. The entire experimental set-up is given in Figure 2. The micro heat sink (a) is supplied by a fluid current pumped, through a 140 mL syringe, by a pumping engine, model Landgraff LA-800 (b). The syringe is clad by an aluminium case, aimed to contain any expansion or compression due to pressure variations. The operating range of the syringe motor has a lower limit of about 113 µl/h and a maximum of 240 ml/min, with an error at the fourth value digit. The serpentine is placed on a hot plate, model Stuart US-150 (c), playing the role of heat source. In the present experiments, the source temperature is set at 70°C. Through a 4-pin data-logger (d) for measurement with K-type thermocouples, the flow inlet temperature (T_{in}), outlet temperature (T_{out}), and that of the aluminium base (T_w) is measured with a resolution of 0.1°C. In order to evaluate pressure drop and efficiency for each fluid mixtures, the Flowplus16-ViscoTec relative pressure sensor (e) is inserted at the inlet of the serpentine. The range of the pressure sensor goes from 70 mbar to 7 bar with an accuracy down to 0.2% of full scale. The inlet fluid temperature has been controlled at the average value of 24°C. Lastly, velocimetry measurements have been carried out through µPIV technique and by a high-speed camera, model Mini FastCam (f). Glass spherical tracers with mean size equal to 15 µm have been used as seeding for all the mixtures. Thus, since Stokes number is inversely proportional to the kinematic viscosity of the mixture [23], its maximum value has been dictated by the least viscous mixture, *i.e.*, that consisting of pure water. This latter mixture is characterized by a Stokes time scale equal to 0.138 µs. Each velocity measurement has been carried out at 30 ml/min, *i.e.,* 0.25 m/s. This flow rate has been chosen because it is within tested intervals for all thermal tests conducted on the five mixtures. Using a partitioned mode of acquisition, with an interval of 1s and using 3000 fps for more than 5000 photos, an analysis time of about 11 seconds for each mixture has been reached. Photo resolution has been fixed at the size of 768x528. Each couple of consecutive frames has been analyzed by cross-correlation algorithms final sub-window size of 16x16 pixels. Results have been filtered by imposing threshold factors of 5 and 3 on local means and standard deviations respectively. Then, points associated with these filtered spurious vectors have been interpolated and filled by smooth processing. Thus, resultant velocity fields errors have been estimated by evaluating the number of filtered and smoothed points in all the analysis domains. The indicated uncertainties vary between 2.5% for high viscous mixtures to values of 6.3% of whole set of analysis points.

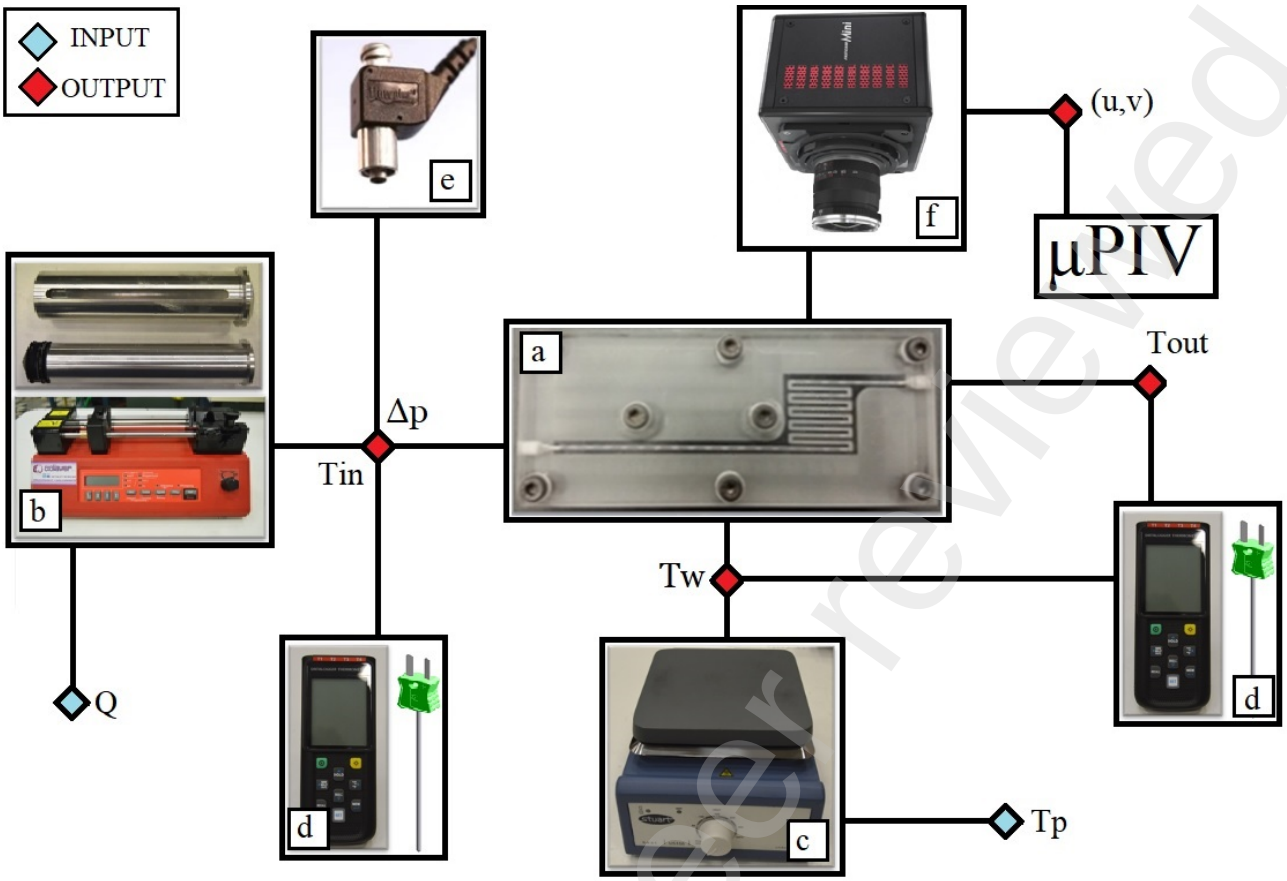

Figure 2: Schematic of the experimental set-up; in details: (a) standard serpentine device, (b) engine pump and syringe, (c) hot plate, (d) data-logger and k-type thermocouple, (e) pressure sensor, (f) high-speed camera.

3. The Choice of Mixtures

The choice of mixture used in present experiments proved to be one of the critical aspects of the work. This selection has been started from the choice of primary fluids which will compose all the carrier mixtures. The latter aspect has been conducted primarily in function of thermofluidic properties and by the chemo-physical compatibility with cell materials. So far, the considered primary fluids are distilled water, alcohol and glycerine. Water is the most common fluid used in microfluidics researches [24]. Its main thermal characteristics are a high value of thermal conductivity and thermal inertia. Glycerine is used as antifreeze and coolant fluid, being also a common by-product of the biodiesel production chain with very low toxicity if compared to ethylene glycol [25]. One of the most interesting thermal properties of liquid glycerine is the large variation of its dynamic viscosity with temperature [26], which is a relevant aspect as it has been illustrated with the Sieder&Tate correlation [18] and with the introduction of Brinkman number [16][22]. Similarly, liquid ethanol alcohol has encountered applications in antifreeze mixtures and as a cooling fluid [27]. It possesses a

high thermal diffusivity coefficient, due to its low thermal inertia. From these three basic fluids, five mixtures are derived as coolants to be employed in experiments on the serpentine micro-cell. Pure water mixture is considered a benchmark for other fluids. A mixture composed of 50% alcohol and 50% distilled water is used due to its high alcohol volumetric concentration, restricted enough to keep a single-phase fluid at 70°C and to avoiding flammability hazard. The third considered mixture consists of 50% glycerine and 50% alcohol in terms of volumetric concentration. Last, two mixtures of distilled water and glycerine are used with 30% and 70% concentrations and vice versa. Each fluid is considered in a specific range of flowrates, due to the resulted different pressure loads imposed by the pump engine. The minimum flow rate is the same for all mixtures and it has been set to 6 ml/min. A fundamental aspect of the analysis on the thermal performance for the different mixtures consists of evaluating all thermal properties parameters. Table 1 lists all relationships used in the present work for computing all the main constitutive parameters of the mixture, starting from the properties of the individual primary fluids (numbered with subscripts 1 and 2). Density and specific heat coefficient are identified by mass and thermal energy balances between final solution and primary fluids, respectively. The mixture dynamic viscosity has been calculated by the Grunberg-Nisan Model [28], under the assumption of no chemical interactions between the two primary fluids. Regarding thermal conductivity, the Filippov and Novoselva relation [29] has been implemented. From these properties illustrated above, it is possible to derive the kinematic and thermal diffusivity coefficients of mixtures. Regarding the dependence of properties on temperature, each primary fluid constitutive parameter is extrapolated by polynomial curve fittings, generated from thermal data tables [26][30][31]. Specific discussion has been followed for the evaluation of the dynamic viscosity thermal dependence due to its exponential trend [28]:

$$\mu(T) = a\, e^{\left(\mathrm{b/T} + cT^2 + dT^2\right)} \tag{1}$$

In equation (1), the constants *a,b,c* and *d* are fixed for each primary fluid. As the temperature varies during the heat exchange process, all thermal properties are evaluated at bulk temperature [21][30], which is the average between the inlet and outlet temperatures:

$$T_{bulk} = 0.5(T_{out} + T_{in}) \tag{2}$$

By the constitutive properties shown above, it has been possible to compute Reynolds and Prandtl numbers [13] for each combination of (mixture, Q):

$$Re(mixture,\ Q) = \frac{Q}{\nu(mixture,\ Q)D} \qquad Pr\ (mixture,\ Q) = \frac{\nu(mixture,\ Q)}{\alpha_T(mixture,\ Q)} \tag{3}$$

Mixture properties	**Relation**
Density	$\rho = x_v\rho_1 + (1 - x_v)\rho_2$
Dynamic viscosity	$ln\,\mu = x_m ln\,\mu_1 + (1 - x_m) ln\,\mu_2$ [29]
Thermal conductivity	$\lambda = x_m\lambda_1 + (1 - x_m)\lambda_2 - 0.72x_m(1 - x_m)\lvert\lambda_1 - \lambda_2\rvert$ [30]
Specific heat coeffcient	$c_p = x_m c_{p1} + (1 - x_m)c_{p2}$
Thermal diffusivity	$\alpha_t = \lambda/c_p\rho$
Kinetic viscosity	$\nu = \mu/\rho$

Table 1: Relations for the evaluation of mixture thermal properties

From these two numbers it is achievable to introduce the Graetz number [21]:

$$Gz = \frac{D}{L} Re\ Pr \tag{4}$$

By the introduction of such dimensionless groups, it is possible to identify all experimental tests in the (*Re, Pr*) diagram, as displayed in Figure 3. Despite having different Reynolds and Prandtl ranges, the various mixtures present the product *Re Pr* similar between each other, which is equivalent to have the same Graetz number and therefore comparable Nusselt numbers [18].

4. Analytical methods

The average Nusselt number is evaluated according to the guidelines outlined by Morini and Yang [21], by the following equation:

$$Nu = \frac{c_p\rho Q(T_\infty - T_{in})D}{\lambda A(T_w - T_{bulk})} \tag{5}$$

The outlet temperature term present in equation (5) is not directly measured and it is derived from cooling thermal transient through a curve fitting model, accordingly to the analytical form of first-order transients [1]:

$$T_{out}(t) = T_\infty + (T_w - T_\infty)\exp(-t/\tau) \quad (6)$$

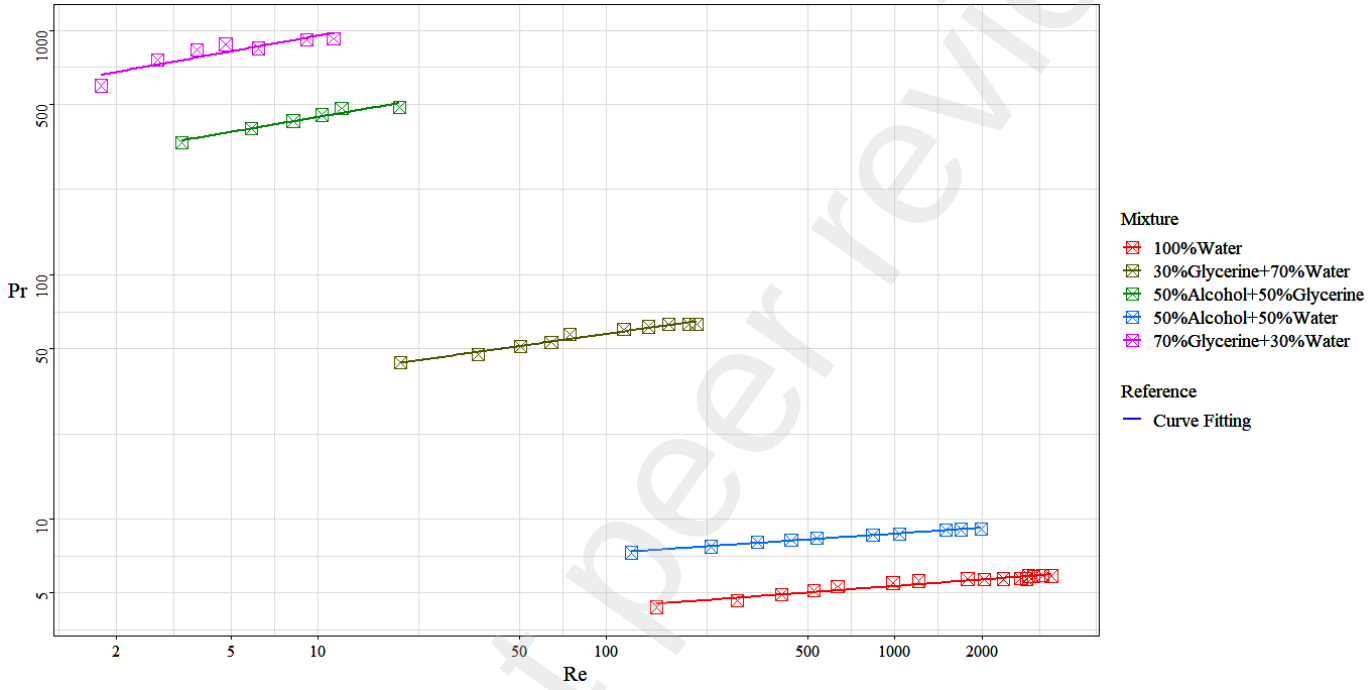

Figure 3: Reynolds-Prandtl number diagram resulting from the experimental campaign for each mixture

From this, it is possible to extrapolate the equilibrium temperature, *i.e.*, the asymptotic temperature T_∞, which is the one included in the Nusselt number calculation illustrated above.

These Nusselt number results are compared to the aforementioned Sieder&Tate [18] correlation:

$$Nu = 1.86\left(\frac{D}{L}Re\,Pr\right)^{\frac{1}{3}}\left[\frac{\mu(T_{bulk})}{\mu(T_w)}\right]^{0.14} = 1.86Gz^{\frac{1}{3}}\left(\frac{\mu_{bulk}}{\mu_w}\right)^{0.14} \quad (7)$$

Therefore, the next step consists of identifying the type of *Nu*-correlation and the involved dimensionless groups, intended as its regressors. Introducing the Brinkman number as the dimensionless ratio between thermal energy generated by viscous dissipation and the conduction of heat from the wall [16]:

$$Br = \frac{\mu u_0^2}{\lambda (T_w - T_{bulk})} \tag{8}$$

it is possible to set the generic correlation of the Nusselt number as a function of the three quantities *(Re, Pr, Br)* by following Buckingham's theorem [13][22] plus the viscosity ratio μ_{bulk}/μ_w introduced by Sieder&Tate [18]:

$$Nu = \alpha\, Re^{\beta}\, Pr^{\gamma} Br^{\delta} \left(\frac{\mu_{bulk}}{\mu_w}\right)^{\eta} \tag{9}$$

To determine the correlation parameters, relation (9) has been linearized and coefficients identified by multivariate linear regression:

$$log\,(Nu) = log\,(\alpha) + \beta log\,(Re) + \gamma log\,(Pr) + \delta log\,(Br) + \eta log\left(\frac{\mu_{bulk}}{\mu_w}\right) \tag{10}$$

The four regressors have not trained the fitting correlation all together. Brinkman number is used coupled with either *Re* or *Re* and *Pr* and these correspond to imposing the conditions of $\gamma = \eta = 0$ or simply $\eta = 0$. Similarly to Sieder&Tate correlation [18] μ_{bulk}/μ_w term trains the regression by just Graetz number, *i.e.*, imposing $\delta = 0$ and $\beta = \gamma$ in equation (10). The purpose of these conditions is aimed at not overestimating the correlation's strength between Nusselt number and viscosity. In fact, this latter is already present in all four regressors *Re, Pr, Br* and μ_{bulk}/μ_w. Otherwise, Reynolds number has been always used in the training of equation (10) since the other considered experimental variable has been the flow rate.

Once Nusselt number has been obtained, it is necessary to evaluate the friction factor in order to carry out an evaluation of thermal efficiency [9][10][32]. Thus, pressure measurements and friction factor can be evaluated by the following definition [33][34]:

$$f = \frac{D}{L}\frac{2\Delta p}{\rho u_0^2} = \frac{D^5 2\Delta p}{L\,\rho Q^2} \tag{11}$$

Considering the axial velocity distribution that is instilled in the laminar regime within rectangular-section channels [35], the theoretical reference for comparison of friction factor results can be identified as follows:

$$u(y,z) = \frac{4D^2\Delta p}{\pi^3 \mu L} \sum_{\substack{k=2h+1 \\ h=0}}^{\infty} \frac{1}{k^3}\left[1 - \frac{\cosh\left(\frac{k\pi y}{d}\right)}{\cosh\left(\frac{k\pi}{2}\right)}\right]\sin\left(\frac{k\pi z}{d}\right) \quad (12)$$

$$Q = \int_{-\frac{d}{2}}^{\frac{d}{2}}\int_{0}^{d} u(u,z)dzdy = \frac{D^4\Delta p}{12\mu L}\left[1 - \frac{192}{\pi^5}\sum_{\substack{k=2h+1 \\ h=0}}^{\infty}\frac{1}{k^5}\tanh\left(\frac{k\pi}{2}\right)\right] \approx 0.0351\frac{D^4\Delta p}{\mu L} \quad (13)$$

$$f = \frac{56.9}{Re} \quad (14)$$

Then, the final step remains evaluating thermal efficiency as the ratio between the parameter quantifying useful thermal effects, *i.e.* Nusselt number, and the one representing the energy losses, *i.e.,* friction factor [10][11]:

$$\varepsilon(Re,Pr,Br) = \frac{Nu(Re,Pr,Br)}{f(Re)} \qquad \varepsilon'(Re,Pr,Br) = \frac{Nu(Re,Pr,Br)}{f(Re)^{\frac{1}{3}}} \quad (15)$$

The left-hand equation (15) has been carried out by considering micro-serpentine efficiency as the linear relationship between useful thermal benefits and energy costs [11]. Second definition of efficiency ε' has been determined by conducting an energy balance as shown by Pongjet [32].

Measurements of the velocity vector field in the small scale-device have been performed by µPIV technique. The detail of the serpentine in which the velocimetry measurements have been taken corresponds to the two last U-shape bends before the straight outlet channel. These sections have been selected to highlight differences in such strongly recirculating regions, in which the five texted mixtures exhibit major differences. For each point within this 2D-analysis region, a collection of *N* instantaneous velocity fields is obtained from *N+1* frames acquired with a certain value of *fps*. Average fields of velocity components *u, v*, magnitude *m* and vorticity orthogonal component ω are computed. Thus, temporal representativeness of average fields is differentiated by zone to highlight possible local turbulence phenomena which contribute to heat transfer.

5. Results and discussion

The evaluation of *(Re, Pr, Br, Nu)* has been strongly influenced by the assessment of constitutive parameters of the carrier mixtures. Therefore, uncertainty propagation on such dimensionless parameters has had to include also all the errors connected to thermal properties computation. This last aspect has been carried out by considering fitting error of constitutive parameters with uncertainty of temperature measurements. Figure 4 shows relative uncertainty values for each mixture. Glycerine mixtures present a higher uncertainty level due to the greater thermal variability that dynamic viscosity exhibits compared to the other constitutive properties as shown by equation (1).

5.1 Nusselt numbers comparison

The first result concerns with the evaluation of Nusselt number as given in Figure 5, where this is presented as a function of Reynolds and Prandtl numbers.

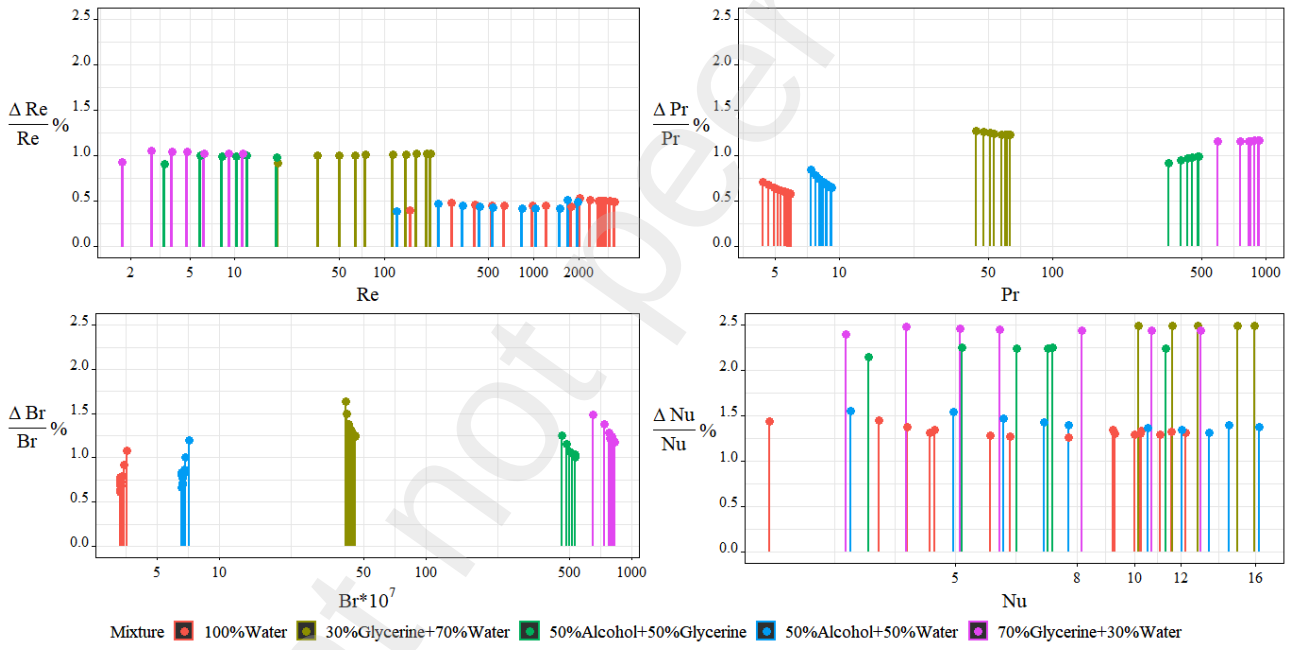

Figure 4: Experimental uncertainty propagation associated to Reynolds, Prandtl, Brinkman and Nusselt numbers.

For all mixtures *Nu*-trends are linear in log-log plot, in agreement with prediction (9) for both dimensionless groups considered as independent variables. Table 2 displays the ratio values between the extent of the variability ranges of *Re, Pr, Gz, Br* and *Nu* for each mixture. *100%Water* and *50%Alcohol+50%Water* present higher average slope $\Delta Nu/\Delta Pr$ compered to glycerine mixtures. This latter aspect is due to the limited variability range of Prandtl number which these two solutions exhibit. In fact, *Nu-Pr* trends for *100%Water* and *50%Alcohol+50%Water* result as they would be

vertical lines when compared with glycerine mixtures trends. Thus, *Nu*-variability for these low-viscosity mixtures is manly related to the variation in Reynolds number. On the other hand, glycerine mixtures exhibit $\Delta Re/\Delta Pr$-values consistently larger than $\Delta Pr/\Delta Re$-results associated to *100%Water* and *50%Alcohol+50%Water.* In fact, *Re* is the dimensionless group representative of the level of flow rate within the channel, which is the second main experimental parameter for all the mixtures. Therefore, Reynolds number results to be an important factor in heat transfer evaluation even for these mixtures in which viscous terms play a predominant role in Nusselt number determination. Additionally, since Reynolds number can be controlled easily by setting flow rate, it is convenient to follow a comparison of the mixtures results in terms of this dimensionless group. So far, Figure 6 illustrates the trend of the coefficients of the log-linear regression between *Nu* and *Re*, identified by the maximum Prandtl number associated with each mixture. The most evident aspect that emerges is the increase in the coefficients of the *Nu*-trend as the viscosity of the mixture increases.

Mixture	$\Delta Pr/\Delta Re$	$\Delta Nu/\Delta Re$	$\Delta Nu/\Delta Pr$	$\Delta Nu/\Delta Gz$	$\Delta Br/\Delta Re * 10^7$
100%Water	$4.50 * 10^{-4}$	$2.59*10^{-3}$	5.75	0.13	$1.79*10^{-2}$
50%Alcohol+50%Water	$9.82 * 10^{-4}$	$6.92*10^{-3}$	7.05	0.22	$2.58*10^{-2}$
30%Glycerine+70%Water	0.10	$6.91*10^{-2}$	0.67	0.32	1.14
50%Alcohol+50%Glycerine	8.57	0.49	$5.72*10^{-2}$	0.28	24.5
70%Glycerine+30%Water	34.7	1.01	$2.91*10^{-2}$	0.30	124

Table *2*: Variability ranges of dimensionless groups for each mixture

Intercept trend, α, displays how *Nu*-values present a higher factor completely independent from Reynolds numbers as viscosity of the mixture increases. On the other hand, the logarithmic slope β highlights how mixtures such as *70%Glycerine+30%Water* and *50%Alcohol+50%Glycerine* can potentially achieve higher *Nu*-values than low-viscosity solutions at the same Reynold number. The attainment of high Reynolds and Prandtl numbers at the same time would correspond to presenting no energy and structural limits for pumping high-viscosity mixtures inside the serpentine channel.

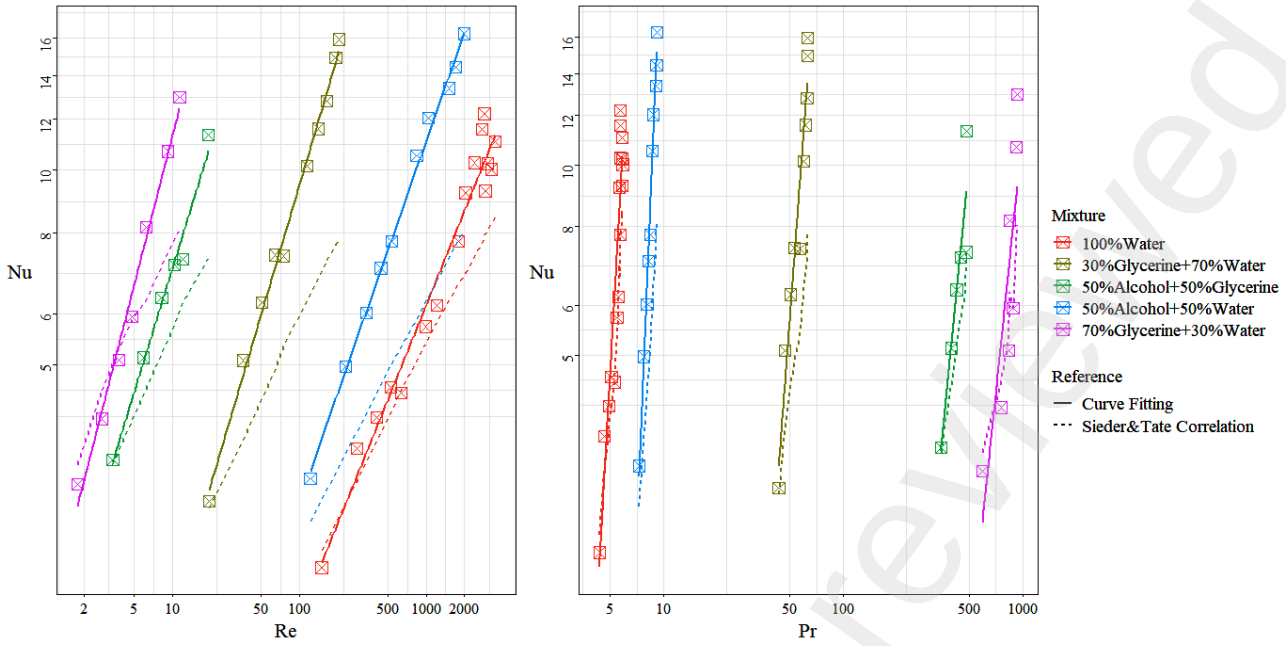

Figure 5: Measured Nusselt number as a function of Reynolds (left) and Prandtl numbers (right); results are compared with Sieder&Tate correlation [18] for each mixture.

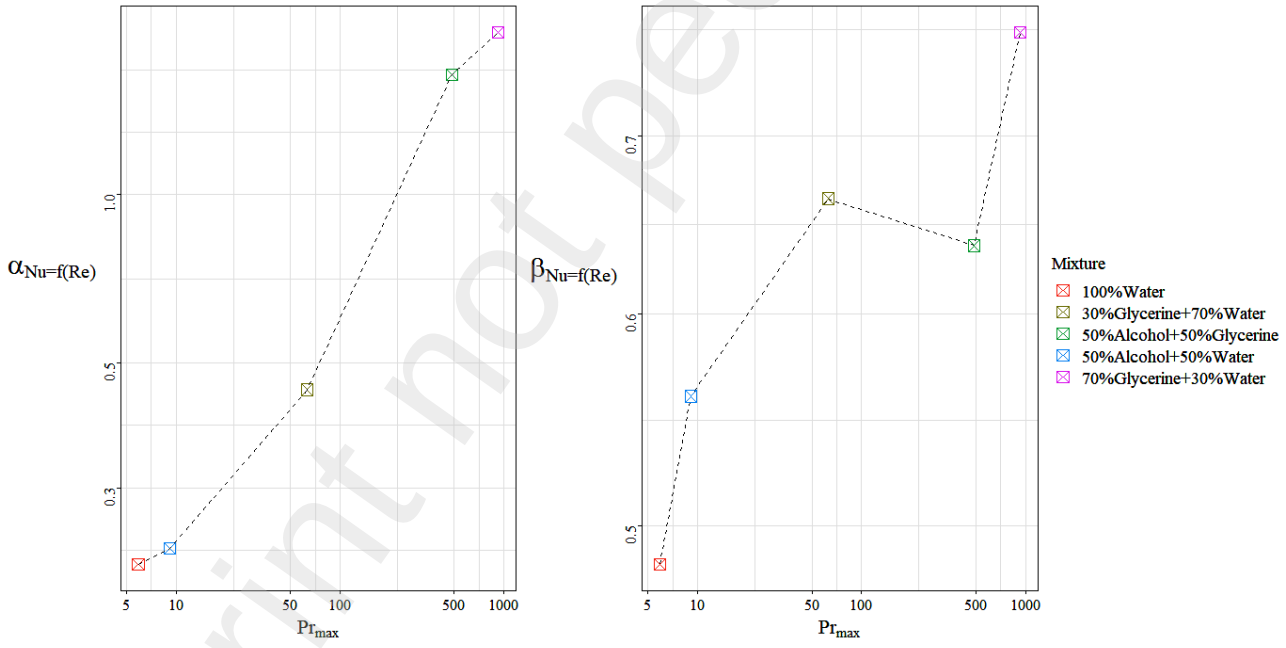

Figure 6: Coefficients in $log(Nu) = log(\alpha) + \beta log(Re)$ relation as a function of the maximum Prandtl number reached by each mixture during the measurements.

Actually, *Re*-increasement promotes viscous dissipation which would become an additional thermal source [23] within the serpentine. Thus, viscous heat generation can rise carrier fluid temperature without any cooling benefits for the heated walls. This latter aspect would imply of measuring a higher difference between outlet and inlet temperatures and then virtually larger Nusselt number [36][37]. This bias on *Nu*-estimation can be identifying through Brinkman number as shown above

in equation (8). Figure 7 shows previous results in terms of Brinkman number in which *Nu-Br* and *Br-Re* trends have log-linear outline [22]. Table 2 highlights how considered mixtures present such a different ranges of Brinkman number. Considering the conventionally threshold for viscous thermal effects in mini and micro-devices at the value of 0.005 [38], it is possible to neglect viscous heat contribute in the considered experimental ranges. Thus, outlet temperature measures and then Nusselt number evaluation have been not altered by viscous dissipation. However, for mixture like *70%Glycerine+30%Water* increasing Reynolds number could implicate reaching *Br*-values large enough to exceed negligence threshold of viscous dissipation effects [21]. Moreover, high levels of viscosity dissipation could warm up cooling fluid at superior temperatures than the heated wall one and thus generating negative Nusselt numbers [22]. Therefore, the exploitation of solutions such *70%Glycerine+30%Water* and *50%Alcohol+50%Glycerine* as cooling fluid for higher Reynolds numbers presents restrictions dictated not only by pumping-system capacity but also from Brinkman number.

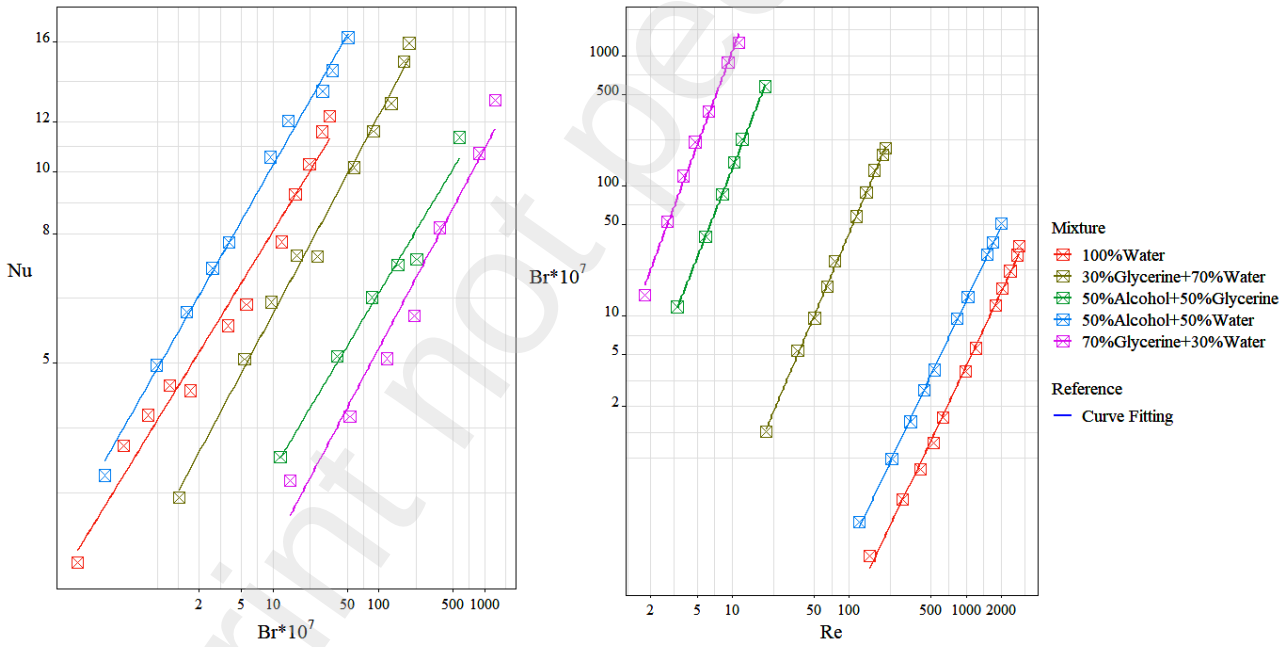

Figure 7: Average Nusselt number computed from experiments as a function of Brinkman number (left) and the experimental domain *Re-Br* (right).

The two plots in Figure 5 can be summarized using the Graetz number as a reference, as carried out in Figure 8. The use of Graetz number allows an easier comparison of Nusselt numbers obtained for the different mixtures. As Table 2 displays, *Gz*-ranges are comparable between different mixtures.

50%Alcohol+50%Water and *30%Glycerine+70%Water* are the two mixtures with the highest Nusselt number for each Graetz one. This result can be explained by the fact that these two solutions present a compromise between Reynolds numbers and viscous values, which contribute to the magnitude of resalted Nusselt number [18][21]. Furthermore, plots in Figure 8 clearly show an increasing divergence between Sieder&Tate relationship [18] and present data. To explain these differences, it should be noted that an important assumption for the validity of the aforementioned correlation consists of the establishment of fully developed thermofluidic conditions. This significant feature is quantified by the values of Graetz number in internal forced convection processes. In fact, values of Gz>10 do not imply vanishing entrance effects in thermal analysis [21]. Since divergence with correlation [18] observed in Figure 8 increases as Graetz number increases, this can therefore be related to the increasing length required for the temperature profile to get fully developed conditions. Also, the thermal profile gradient evaluated at the wall is then much higher in the developing region [30] thus, the associated Nusselt numbers will be larger when compared to a condition in which thermal profile is completely developed. This latter explains why higher Nusselt number magnitude have been obtained, as in results by Morini [21].

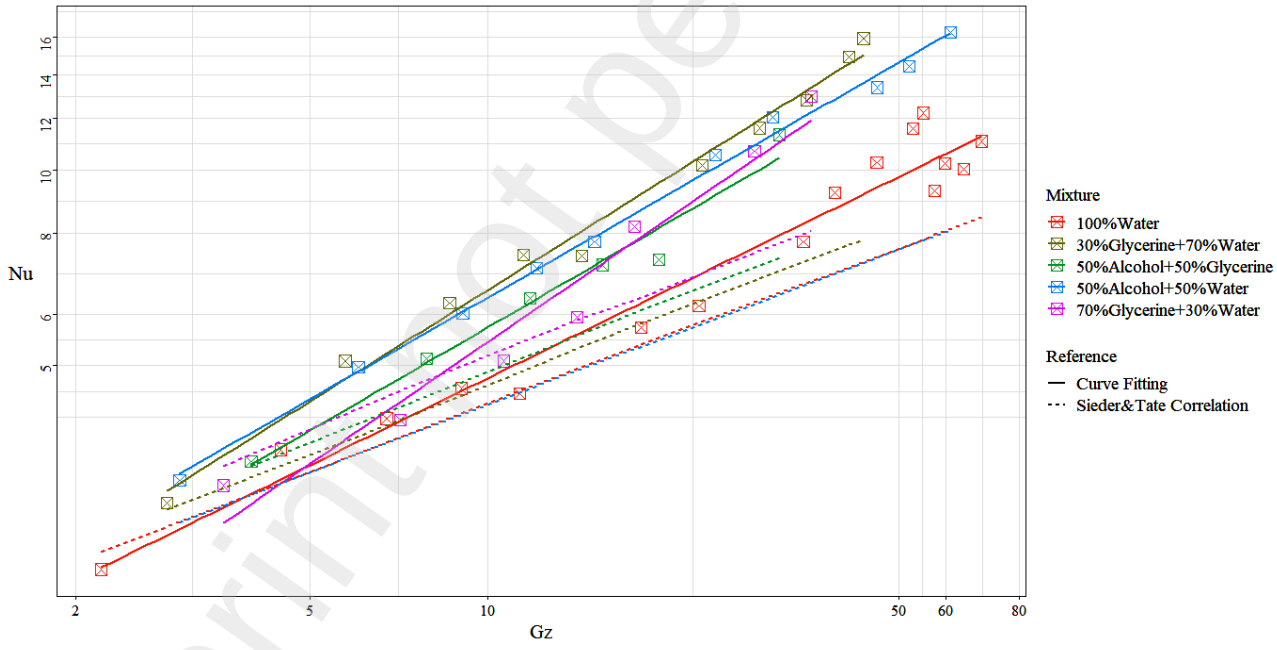

Figure 8: Measured Nusselt number as a function of Graetz number; results are compared with Sieder&Tate correlation [18] for each mixture

Mixture	Model	α	β	R^2	σ_{rms}
	$\alpha\, Gz^{\beta}$				

100%Water	1.722	0.443	0.962	0.840
50%Alcohol+50%Water	1.929	0.518	0.996	0.368
30%Glycerine+70%Water	1.767	0.567	0.990	0.458
50%Alcohol+50%Glycerine	1.704	0.526	0.973	0.513
70%Glycerine+30%Water	1.302	0.620	0.961	0.608
	$\alpha\, Re^{\beta}$			
100%Water	0.219	0.484	0.967	0.799
50%Alcohol+50%Water	0.234	0.559	0.996	0.363
30%Glycerine+70%Water	0.448	0.663	0.994	0.343
50%Alcohol+50%Glycerine	1.631	0.637	0.984	0.387
70%Glycerine+30%Water	1.941	0.765	0.987	0.336

Table 3: Statistical estimators of *Nu*-*Gz* and *Nu*-*Re* regressions identified for each mixture

5.2 Nusselt number correlation

Table 3 summarize parameters and performance of single regression applied to one-by-one mixture and shown in the previous plots. As pointed out above, each carrier fluid presents different ranges of Reynolds and Prandtl numbers. However, a more homogeneous training set is obtained to identify a unique *Nu*-correlation, by merging measurements from all mixtures into a single dataset. Table 4 highlights coefficient estimators of various considered log-linear models and their related performance indicators. For correlations in which Brinkman number is considered as a regressor, an increase in the intercept term is obtained compared to the other regressions. This latter aspect is clearly associated with the negligibility of *Br*-values [21] within this experimental range. Furthermore, correlation b) presents a negative estimator for the *Pr*-exponent, which suggests that training of *Nu*-values in terms of Prandtl and Brinkman numbers together has generated overfitting. Thus, Brinkman number has not resulted to be the representative regressor for the viscosity contribution to Nusselt numbers, within the experimental ranges of the present work. Correlation d) has been carried out to fit the empirical form proposed by Sieder&Tate [18]. The total magnitude of intercept and viscous term $\alpha\ (\mu_{bulk}/\mu_w)^{\eta}$ is comparable with $1.86\ (\mu_{bulk}/\mu_w)^{0.14}$ shown in equation (7). The main difference is related to *Gz*-exponent, which turns out to be greater than the one in Sieder&Tate correlation. The latter aspect is clearly connected with aforementioned entrance effects

contribution to Nusselt numbers [21][37]. In terms of performance and explained variance, bivariate regression *Nu=f(Re,Pr)* has been resulted as the best model in the shown domain.

Correlation	α	β	γ	δ	η	R^2	σ_{rms}
a) $Nu = \alpha Re^{\beta} Pr^{\gamma}$	0.103	0.489	0.517	0.000	0.000	0.890	1.59
b) $Nu = \alpha Re^{\beta} Pr^{\gamma} Br^{\delta}$	8357	0.570	-0.180	0.721	0.000	0.897	1.51
c) $Nu = \alpha\ Gz^{\beta} (\mu_{bulk}/\mu_w)^{\eta}$	1.709	0.478	0.478	0.000	0.098	0.869	1.70
d) $Nu = \alpha\ Re^{\beta} Br^{\delta}$	460.9	0.552	0.000	0.538	0.000	0.896	1.53

Table 4: Statistical estimators of *Nu*-regressions

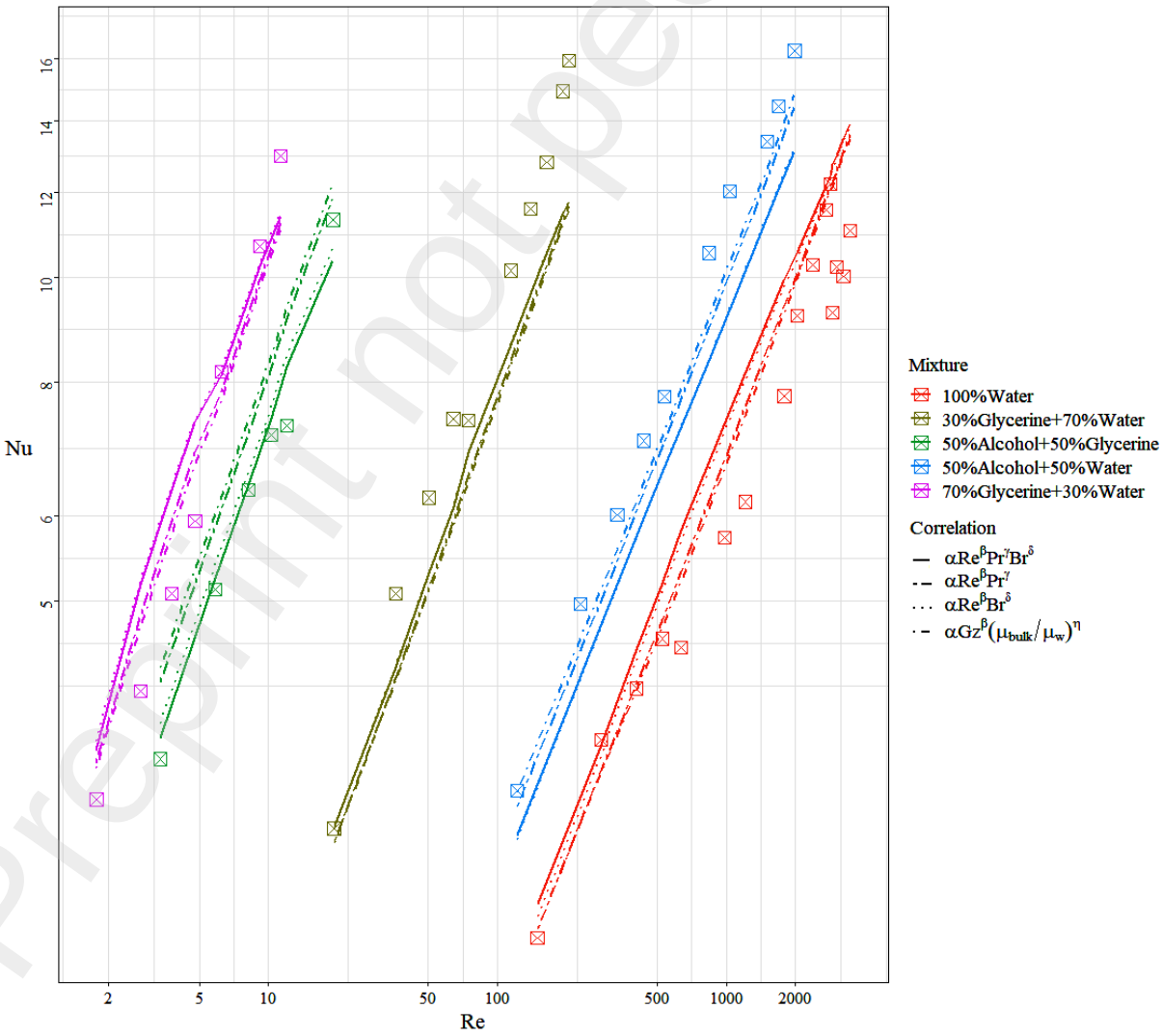

Figure 9: *Nu*-correlations results compared to experimental data for each mixture

5.3 Thermal Efficiency

Figure 10 shows results of pressure drop measured in the serpentine channel for the different mixtures. The plot on the right displays a high degree of log-linear fitting between the flow rate and the corresponding pressure load, a feature that becomes perfectly evident as the dynamic viscosity of the mixture increases. Friction factor plot highlights how glycerine mixtures encounter a better adherence to the theoretical reference [30][35] while the two other mixtures show a great divergence from the latter. From the evaluation of Nusselt number shown above and the results in terms of friction factor, thermal efficiency of the serpentine has been calculated for the different mixtures in the two forms $\varepsilon = Nu/f$ and $\varepsilon' = Nu/f^{0.33}$ and plotted in Figure 11. While the ε - trend clearly penalizes highly viscous mixtures and identifies pure water solution as the most efficient, the results of ε' show that viscous mixtures exhibit high growth rates of efficiency as Reynolds number increases. This larger ε'-gradient is due to the high slope of the *Nu=f(Re)*-curves which *50%Alcohol+50%Glycerine* and *70%Glycerine+30%Water* mixtures present. Therefore, the efficiency trend will also be affected by the negative influence that the Brinkman number implies by increasing the Reynolds number [22]. Thus, both ε' and ε trends indicate the exclusion of these two mixtures in the choice of the cooling fluid with those experimental parameters. The ε' definition awards *50%Alcohol+50%Water* as the best cooling fluid. Since this latter is the mixture with higher Nusselt number than *100%Water,* it is concluded that this mixture can be considered as the best choice to achieve optimal cooling effect with low enough pumping energy expense. It must be pointed out that *50%Alcohol+50%Water* is the one with the lowest boiling point of all, and therefore if one were to increase the temperature of the device to be cooled beyond this level, the evaluation of the constitutive properties of the mixture and consequently all the dimensionless groups would require a different approach, based on the biphasic nature of the fluid.

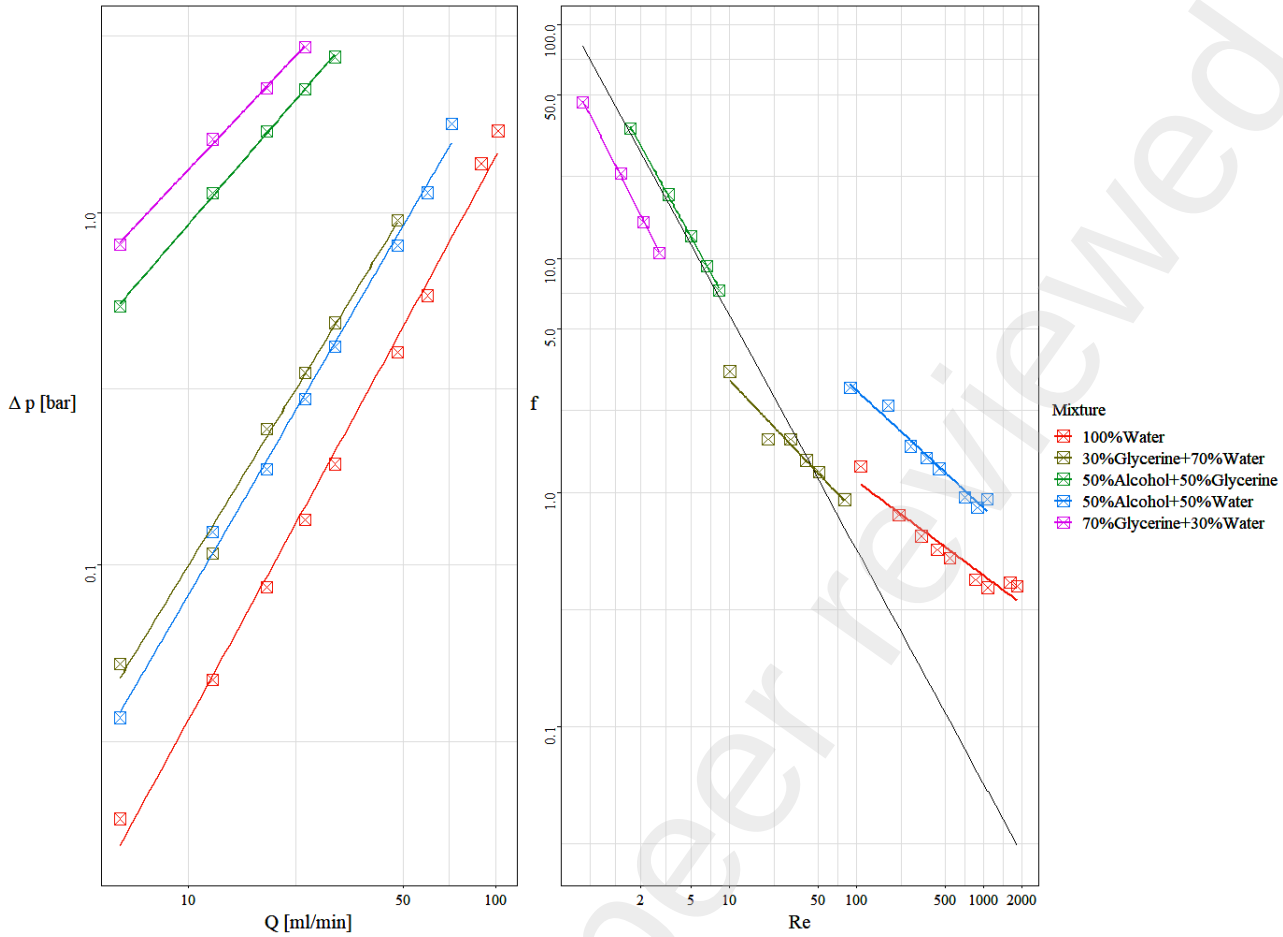

Figure 10: Trend of friction factor as a function of Reynolds number (right) and pressure loads as function of the flowrate; *f*-results are compared with theoretical laminar relation while pressure loads points (left) are plotted with their log-linear curve fittings.

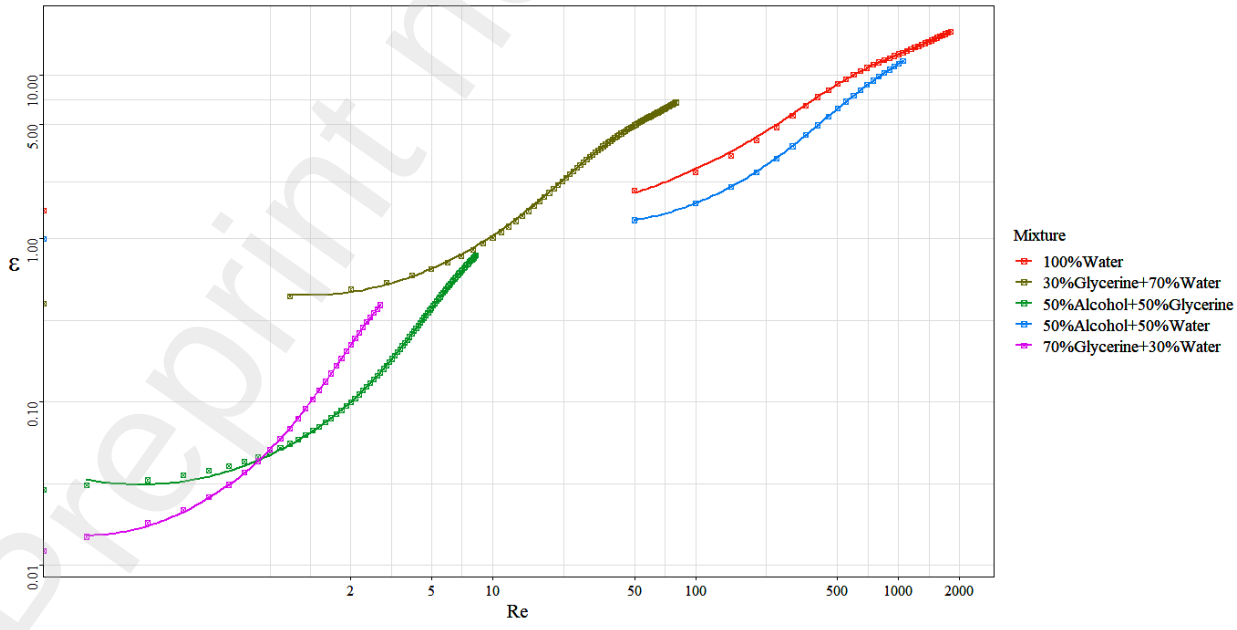

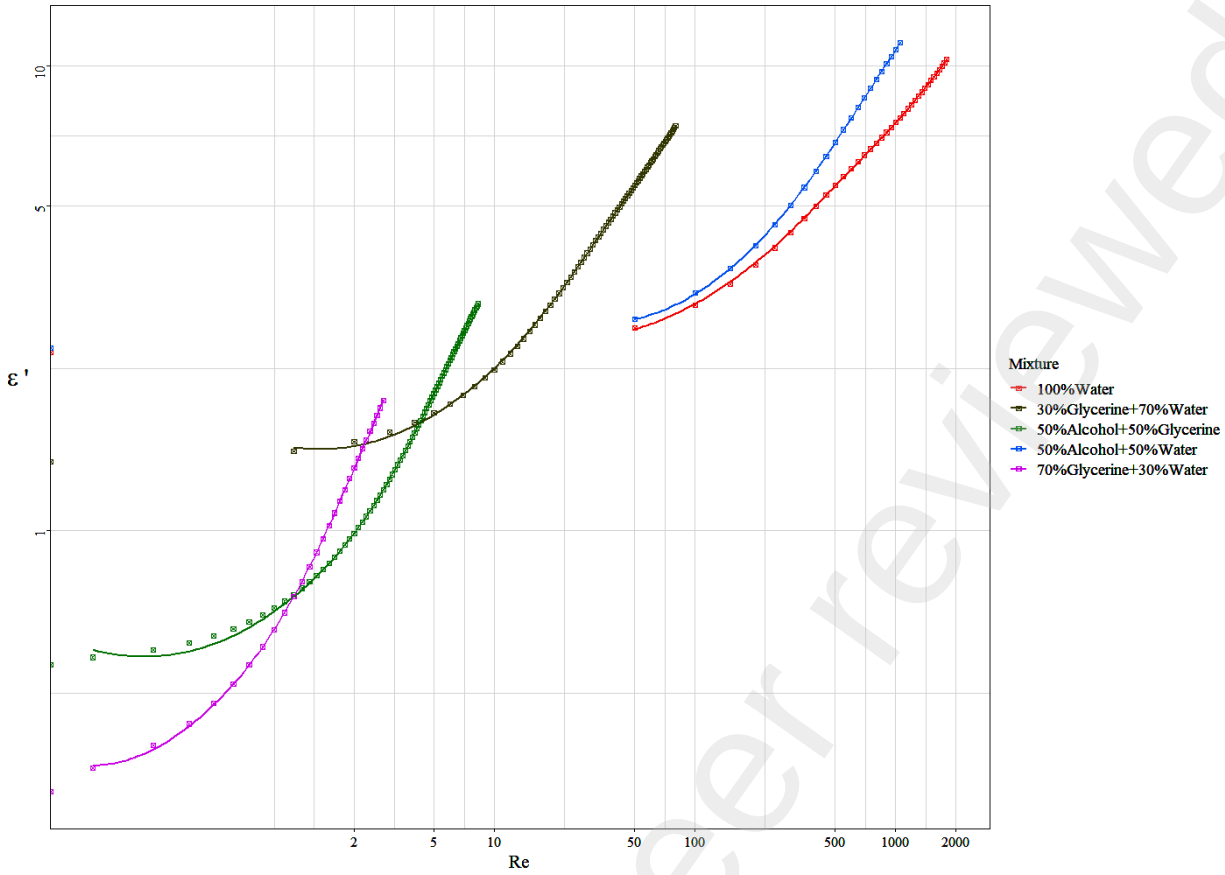

Figure 11: Trends of thermal efficiency definitions as function of Reynolds number for each mixture

5.4 Velocimetry results

As shown above, for low-viscosity mixtures the most important factor in assessing Nusselt number and thus thermal efficiency is the Reynolds number. In fact, this dimensionless group is used to identify the type of fluid-dynamic regime (laminar, transitional, turbulent) of the flow [30]. Although measurements have been carried out mainly in the laminar regime, this aspect does not exclude the possible presence of local three-dimensional and turbulent phenomena which promote internal convection by increasing mixing phenomena. Thus, velocity field measurements are presented to correlate local turbulence, Reynolds number and its influence on Nusselt number. Figure 12 displays the average magnitude, vectors and vorticity fields obtained with a flow rate of 30 ml/min. Velocity magnitude maps of the glycerine flows exhibit continuity in magnitude along the two bends, whereas this does not occur for those fluids which have reached higher Reynolds values, *i.e.* with lower viscosity. It is supposed that this is due to strongly three-dimensional turbulent motions. However, the analysis of such phenomenon has been conducted using a dimensionless mean velocity scatterplot, in which mean fields of the absolute components are normalized by the mean velocity magnitude m (u/m, v/m), as plotted in Figure 13. Each point of these scatterplots is placed at a distance from the origin equal to $R = \sqrt{(u/m)^2 + (v/m)^2} = M/m$, where $M = \sqrt{u^2 + v^2}$ is a virtual magnitude which

would be obtained by the average components. In general, divergence between mean velocity magnitude *m* and the magnitude of mean components *M* increases as the associated standard deviation and thus temporal fluctuations increase. So far, the scatterplots presented in Figure 13 give indication of the presence of local turbulence. Comparing results obtained with the different mixtures in bends and inversion regions, represented in red and blue colours respectively, it is clear that those associated with low viscosity present very sparse scatterplots. On the other hand, for *70%Glycerine+30%Water* and *50%Alcohol+50%Glycerine* results are much closer to the unity circle, which implies negligible local fluctuations. This aspect indicates the presence of localized turbulent effects in those bend regions with a strongly three-dimensional characterization [11][30]. Such turbulence and three-dimensionality localized in the U-Shape regions just promote mixing and diffusion phenomena, including heat transfer [1]. This explains why for low-viscosity mixture Reynolds number represents the main regressor in *Nu*-correlations with the lowest intercepts, as shown in Table 3. Considering the straight sections, in green in the figure, a negligible dispersion is observed except for some point located at the boundaries. For high-viscosity mixtures, the dispersion can be considered almost equal to zero. This latter aspect can be also noticed from vorticity maps of Figure 12 and by the transversal vorticity profiles in Figure 14, in which a decrease in Reynolds number leads to increases of flow laminarity. Since standard serpentine configuration is composed of multiply bends-inversion regions, the effect of the local turbulence on thermal performance becomes such as the main factor for low-viscosity mixture. Therefore, this latter aspect explains why standard serpentine geometry has been identified to be the most efficient in previous studies [11] by using pure water as carrier fluid.

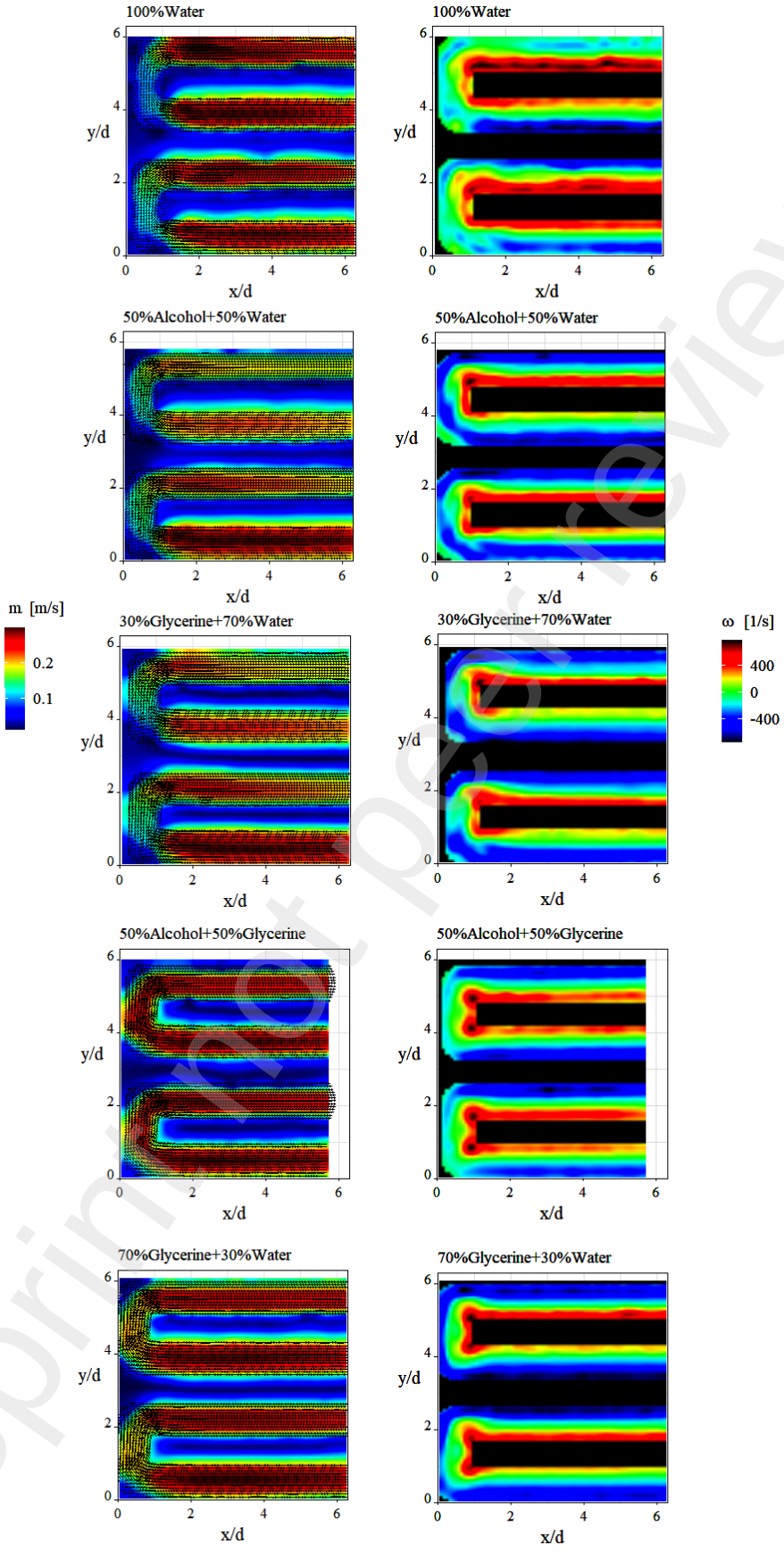

Figure 12: Mean velocity magnitude and vorticity results for each mixture

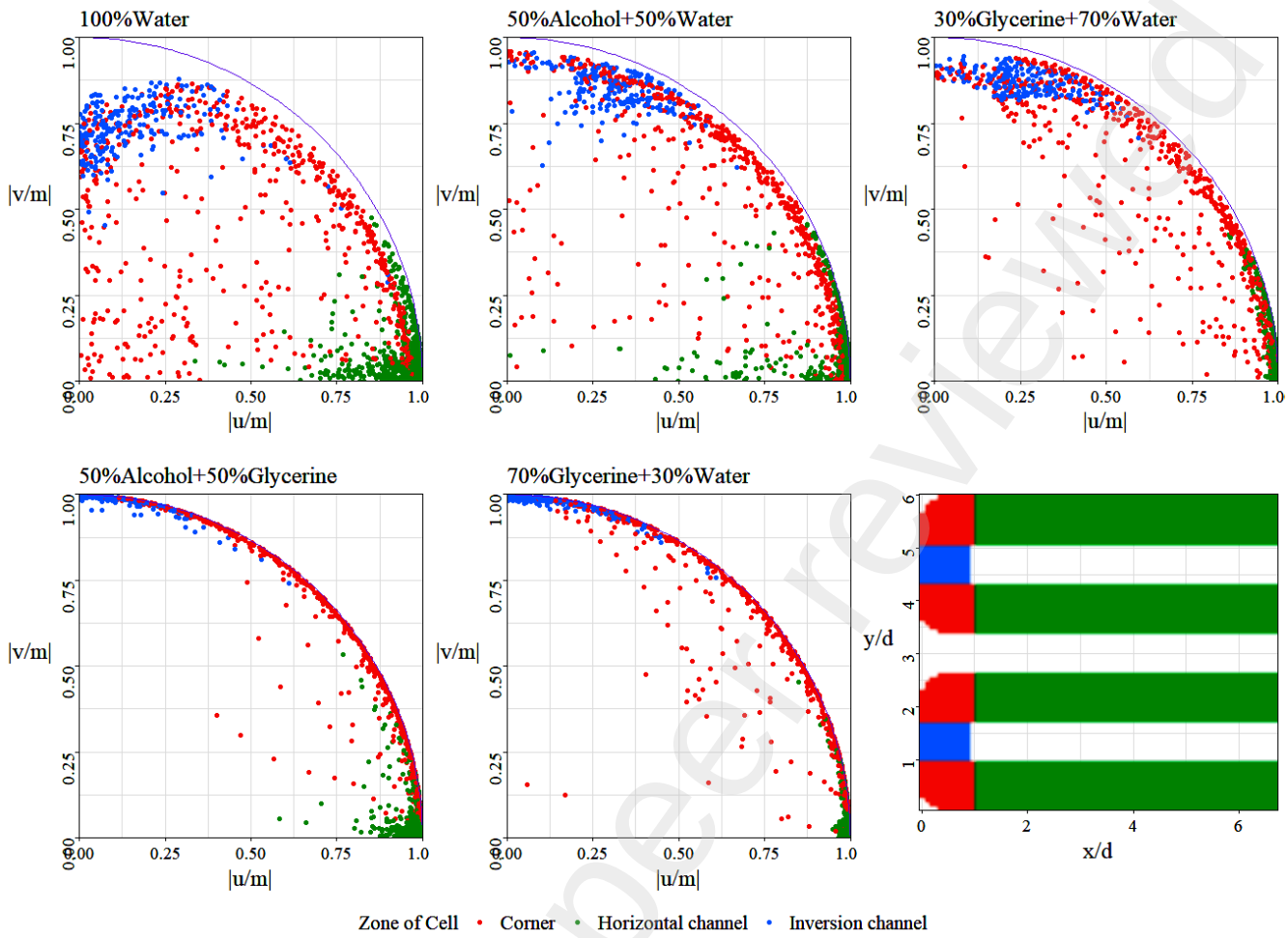

Figure 13: Mean dimensionless velocity scatterplots parametrized in terms of acquisition regions.

6. Conclusion

In the presented work, the analysis on a microfluidic device consisting of a standard serpentine channel has been conducted with five different types of cooling fluid. The identified and obtained results can be summarized in the following manner:

- Viscous properties of mixtures and their variability with temperature appear to be relevant factors in determining the performance of the micro-fluidic device, especially for glycerine coolants.

- In the chosen flow rate range for each mixture, viscous dissipation has not resulted as significant undesired heat source. Thus, the outlet temperatures of each mixture have not been increased by viscous friction, as the obtained Nusselt numbers.

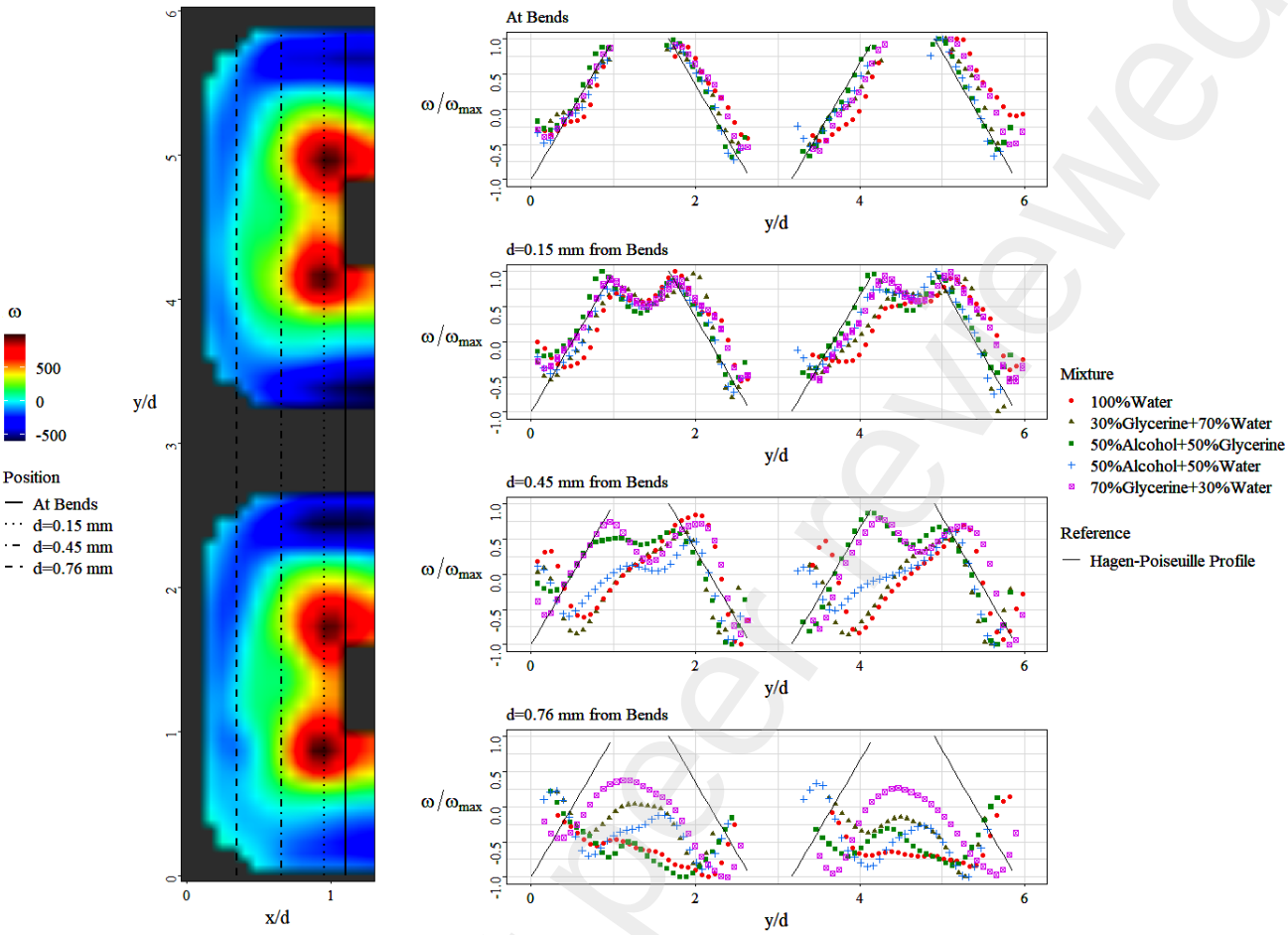

Figure 14: Mean vorticity field at bends for *50%Alcohol+50%Glycerine* (left) and vorticity profile (right) parametrized by mixture and distance from bends

- High-viscosity mixtures such as *70%Glycerine+30%Water* and *50%Alcohol+50%Glycerine*, have exhibited high Nusselt numbers for low flow rates. Although these mixtures exhibit the highest slopes of *Nu-Re* trends, increasing Reynolds number would imply increasing Brinkman number at values where the effects of viscous dissipation cannot be neglected.

- The experimental data presented a divergence from Sieder&Tate correlation as Graetz number increases *i.e.*, as the importance of entrance effects for thermo-hydraulic development rises.

- In determining a *Nu*-correlation, the best model has been identified in the bivariate *Nu=f(Re, Pr)*. In particular, the application of this correlation presents greater performance for high-viscosity mixtures, whereas for those mixtures with higher Reynolds numbers, Nusselt numbers are optimally correlated also with the only use of Reynolds numbers.

- Efficiency trends have showed *50%Alcohol+50%Water* results to be the best choice as coolant into the micro-serpentine. Otherwise, if there were no operational limits to fluid pumping, *30%Glycerine+70%Water* has been identified the one with the highest values of Nusselt numbers.

- Velocimetry has made possible to correlate the importance of Reynolds number with Nusselt number for mixtures like *50%Alcohol+50%Water* and *100%Water*, by identifying the presence of local turbulence. These effects contribute to convective heat transfer by increasing the flow mixing.

In conclusion, given the wide use of microfluidic devices in laminar regime due to their optimal thermal performance comparable even to conventional systems in turbulent regime [39], fluid viscosity results to be a key factor in understanding thermal efficiency of such heat sinks.

Conflict of interest

None.

Acknowledgment

The authors would like to thank Alessandro Caterina, Maximo Orlando Capponi and Antonello Binni for the help in measurement set-up and cell manufacturing.

Funding sources

This research did not receive any specific grant from funding agencies in the public, commercial, or not-for-profit sectors.

References

[1] M. Mahmoud, Engineering Thermofluids-Thermodynamics, Fluid Mechanics and Heat Transfer, first ed., Springer, Berlin, 2005, pp. 520.

[2] Pfahler, J., J. Harley, H. Bau and J. Zemel , Liquid transport in micron and submicron channels, Sensors and Actuators A: Physical 22, 1990, pp. 431–434.

[3] Mehendale SS, Jacobi AM, Shah RK. Fluid flow and heat transfer at micro-and meso-scale with application to heat exchanger design, ASME. Appl Mech Rev. 2000, pp. 175-193.

[4] Kandlikar SG, Grande WJ, Evolution of microchannel flow passages: thermohydraulic performance and fabrication technology, International Mechanical Engineering Congress and Exposition, 2002, pp. 59-72.

[5] Li, Z., Y. L. He, G. H. Tang and W. Q. Tao Experimental and numerical studies of liquid flow and heat transfer in microtubes. International journal of heat and mass transfer 50, 2007, pp. 3447–3460.

[6] J. Zhang, P.T. Lin, Y. Jaluria, Design and optimization of multiple microchannel heat transfer systems, Journal of Thermal Science and Engineering Applications, 2014, pp. 14.

[7] Y. Sui, P.S. Lee, C.J. Teo, An experimental study of flow friction and heat transfer in wavy microchannels with rectangular cross section, International Journal of Thermal Sciences 50, 2011, pp. 2473-2482.

[8] X. Hao, B. Peng, G. Xie, Y. Chen, Thermal analysis and experimental validation of laminar heat transfer and pressure drop in serpentine channel heat sinks for electronic cooling. Journal of Electronic Packaging, 2014, pp. 136.

[9] A. Kumar, M. Kumar, S. Chamoli, Comparative study for thermal-hydraulic performance of circular tube with inserts, Alexandria Engineering Journal 55, 2016, pp. 343–349.

[10] Hamidreza Rastana, Amir Abdi, Bejan Hamawandi, Monika Ignatowicz,Josua P. Meyer, Björn Palma, Heat transfer study of enhanced additively manufactured minichannel heat exchangers, International Journal of Heat and Mass Transfer 161, 2020.

[11] M. Spizzichino, G. Sinibaldi, G.P.Romano, Experimental Investigation on Fluid Mechanics of Micro-Channel Heat Transfer Devices, Exp. Thermal and Fluid Science 118, 2020.

[12] X. Hao, B. Peng, G. Xie, Y. Chen, Thermal Analysis and Experimental Validation of Laminar Heat Transfer and Pressure Drop in Serpentine Channel Heat Sinks for Electronic Cooling, Journal of Electronic Packaging, 2014, pp. 136.

[13] E Buckingham, Model experiments and the forms of empirical equations, Transactions of the ASME, 1915, pp. 263-296.

[14] D. B. Tuckerman, R. F. W. Pease, High-Performance Heat Sinking for VLSI, IEEE Electron Device Letters, 1981.

[15] Peng, X. F. and Peterson, G. P., Convective heat transfer and flow friction for water flow in microchannel structures. International Journal of Heat and Mass Transfer, 1996, pp. 2599-2608.

[16] C. P. Tso, S. P. Mahulikar, Experimental verification of the role of Brinkman number in microchannels using local parameters, International Journal of Heat and Mass Transfer 43, 2000, pp. 1837-1849.

[17] P.S. Lee, D. Liu, S.V. Garimella, Investigation of heat transfer in rectangular microchannels, Int. J. Heat Mass Transfer 48, 2005, pp. 1688-1704.

[18] E.N. Sieder, G.E. Tate, Heat Transfer and Pressure Drop of Liquids in Tubes, Ind. Eng. Chem. 28, 1936, pp. 1429-1435.

[19] Kakac, S., Shah, R. K. and Aung, Handbook of Single-Phase Convective Heat Transfer, John Wiley and Sons, 1987.

[20] Qu, W., Mala, G. M. and Li, D. Q.,"Heat transfer for water flow in trapezoidal silicon microchannels," Int. J. Heat Mass Transfer 43, 2000, pp. 3925-3936.

[21] G.L. Morini, Y. Yang, Guidelines for the Determination of Single-Phase Forced Convection Coefficients in Microchannels, Journal of Heat Transfer 135, 2013, pp. 10.

[22] C.P. Tso, S.P. Mahulikar, The role of the Brinkman number in analysing flow transitions in microchannels, International Journal of Heat and Mass Transfer 42, 1999, pp. 1813-1833.

[23] Brennen, Christopher E, Fundamentals of multiphase flow, Cambridge Univ, 2005.

[24] Ganesan Narendran, Nagarajan Gnanasekaran and Dharmaraj A. Perumal, A Review on Recent Advances in Microchannel Heat Sink Configurations, Recent Patents on Mechanical Engineering, 2018, pp. 190-215.

[25] R. Douglas Hudgens, Richard D. Hercamp, Jaime Francis, Dan A. Nyman Yolanda Bartoli, An Evaluation of Glycerin as a Heavy Engine Antifreeze/Coolant Base, Journal of fuel and lubrification, 2007, pp. 834-849.

[26] Glycrine: an overview, Glyecerine & Oleochemical Division, 1990, pp. 14.

[27] Da Qu, Peng Zhang, Jiadai Xue, Yun Fan, Zuhui Chen, Bo Wang, Experimental Study on the Effects of Coolants on Surface Quality and Mechanical Properties of Micromilled Thin-Walled Elgiloy, 2018.

[28] W. Marczak, N. Adamczyk, Viscosity of Associated Mixtures Approximated by the Grunberg-Nissan Model, International Journal of Thermophysics, 2011.

[29] U. N. Gaitonde, D. D. Deshpande, and S. P. Sukhatme, The Thermal Conductivity of Liquid Mixtures, Ind. Eng. Chem. Fundam., 1978.

[30] Y.A. Cengel, Introduction to Thermodynamics and heat transfer, McGraw-Hill, 2009, pp 553.

[31] A. Kayode Coker, Physical Proprieties of Liquids and Gases, Ludwig's Applied Process Design for Chemical and Petrochemical Plants, 2007, pp. 103-132.

[32] P. Promvonge, Thermal augmentation in circular tube with twisted tape and wire coil turbulators, Energy Conversion and Management, 2008, pp. 2949–2955.

[33] W.M. Abed, R.D. Whalley, D.J.C. Dennis, R.J. Poole, Numerical and experimental investigation of heat transfer and fluid flow characteristics in a micro-scale serpentine channel, International Journal of Heat and Mass Transfer 88, 2015, pp. 790-802.

[34] J.T. Fanning, Hydraulic Engineering and Manual for Water Supply Engineers, D. Van Nostrand, 1882.

[35] Henrik Bruus, Theroretical microfluidics, Technical University of Denmark, 2006.

[36] C. P. Tso, S. P. Mahulikar, The use of the Brinkman number for single-phase forced convective heat transfer in microchannels, International Journal of Heat and Mass Transfer 41, 1997.

[37] Guo, Z. Y., and Li, Z. X., "Size Effect on Microscale Single-Phase Flow and Heat Transfer," Int. J. Heat Mass Transfer 46, 2003, pp. 149–159.

[38] Morini, G. L., and Spiga, M., "The Role of Viscous Dissipation in Heated Microchannels," ASME J. Heat Transfer 12, 2007, pp. 308–318.

[39] Tuckermann, D. B. and Pease, R. F., Optimized convective cooling using micromachined structure. Journalof the Electrochemical Society, 1982.